ADVANCED ELECTRONIC MATERIALS
www.advelectronicmat.de

Sulfurization Engineering of One-Step Low-Temperature MoS_2 and WS_2 Thin Films for Memristor Device Applications

*Yuqian Gu, Martha I. Serna, Sivasakthya Mohan, Alejandra Londoño-Calderon, Taimur Ahmed, Yifu Huang, Jack Lee, Sumeet Walia, Michael T. Pettes, Kenneth M. Liechti, and Deji Akinwande**

2D materials have been of considerable interest as new materials for device applications. Non-volatile resistive switching applications of MoS_2 and WS_2 have been previously demonstrated; however, these applications are dramatically limited by high temperatures and extended times needed for the large-area synthesis of 2D materials on crystalline substrates. The experimental results demonstrate a one-step sulfurization method to synthesize MoS_2 and WS_2 at 550 °C in 15 min on sapphire wafers. Furthermore, a large area transfer of the synthesized thin films to SiO_2/Si substrates is achieved. Following this, MoS_2 and WS_2 memristors are fabricated that exhibit stable non-volatile switching and a satisfactory large on/off current ratio (10^3–10^5) with good uniformity. Tuning the sulfurization parameters (temperature and metal precursor thickness) is found to be a straightforward and effective strategy to improve the performance of the memristors. The demonstration of large-scale MoS_2 and WS_2 memristors with a one-step low-temperature sulfurization method with simple strategy to tuning can lead to potential applications such as flexible memory and neuromorphic computing.

1. Introduction

In 2018, the semiconductor industry surpassed the 10-nm threshold to the 7-nm technology node, with the 5 and 3-nm nodes prepared for the following years.[1] With several challenges in scaling-down, in-memory computing as an emerging alternative of traditional von Neumann architecture has attracted extensive research interest, which requires fast and scalable memory devices such as Resistive Random-Access Memory (RRAM), also known as memristors, Phase-Change Memory (PCM), and Magnetoresistive Random-Access Memory (MRAM).[2] Meanwhile, 2D materials have been widely studied, and several applications such as transistors,[3–5] flexible electronics,[6,7] photodetectors,[8,9] and more recently, memristors devices,[10–15] have been demonstrated. Due to the unique properties of 2D materials, memristors based on 2D materials have shown outstanding electrical properties, including high on-off ratio, low switching thresholds (≈100 mV), fast switching speed, ultra-low power consumption (fJ per switching), and THz operation.[14–18]

The emerging applications of 2D materials demand new synthesis and integration processes. Furthermore, to achieve commercial applications, much effort has been devoted to the large-area synthesis[19–21] and patterning[22–24] of 2D materials to ensure the transition of these unique materials from the laboratory to industrial manufacturing. However, most reported studies rely on conventional CVD synthesis,[25] and MOCVD,[26,27] which are mostly relatively high-temperature processes. Due to the dissimilarity of synthesis equipment and complexity of synthesis procedures, a standard and simple process applicable for the industrial manufacturing of wafer-scale 2D materials remains a challenge. As an alternative to conventional CVD, studies have shown that sulfurization of thin metallic films can result in the large-scale synthesis of MoS_2 and WS_2. One of the advantages of sulfurization processes, compared to the conventional CVD method, is large area coverage and uniformity of the as-grown film, due to simultaneously sulfurization over the entire substrate. Recent works have demonstrated synthesis of MoS_2 with vertically aligned layers,[28] sulfurization for horizontally layered MoS_2 with the high-temperature process (above 700 °C),[29,30] and relatively long sulfurization times (more than 1 h).[31]

For this reason, one of the main challenges in sulfurization processes is to use temperatures below 700 °C while achieving horizontally layered films in short processing times. This work successfully demonstrates a simple method to synthesize MoS_2 and WS_2 films via one-step low-temperature sulfurization. The

Y. Gu, M. I. Serna, S. Mohan, Y. Huang, J. Lee, D. Akinwande
Microelectronics Research Center
The University of Texas at Austin
Austin, TX 78758, USA
E-mail: deji@ece.utexas.edu

S. Mohan, K. M. Liechti, D. Akinwande
Materials Science and Engineering Program and Texas Materials Institute
The University of Texas at Austin
Austin, TX 78712, USA

A. Londoño-Calderon, M. T. Pettes
Center for Integrated Nanotechnologies
Materials Physics and Applications Division
Los Alamos National Laboratory
Los Alamos, NM 87545, USA

T. Ahmed, S. Walia
School of Engineering
Department of Electronics and Telecommunications Engineering
Royal Melbourne Institute of Technology
Melbourne, VIC 3000, Australia

The ORCID identification number(s) for the author(s) of this article can be found under https://doi.org/10.1002/aelm.202100515.

DOI: 10.1002/aelm.202100515

samples can be scaled up to wafer scales (2 in. diameter in this work) and then transferred to prepared substrates. As an application of these sulfurized Transition metal dichalcogenide (TMD) films, successful fabrication and operation of memristors are presented, showing stable non-volatile switching and a satisfactory large on/off current ratio (10^3–10^5). Furthermore, we found that tuning the sulfurization parameters (temperature and metal precursor thickness) is a simple yet effective approach to improve the operational characteristics of memristors.

2. Results and Discussions

Figure 1a,b depicts the MoS_2 and WS_2 thin film synthesis procedure and the sulfurization experimental setup. First, molybdenum and tungsten metallic films were deposited by e-beam evaporation onto sapphire substrates, followed by a sulfurization process at 550 °C for 15 min. The specific details of this process are outlined in the Experimental Section. After sulfurization, the films were transferred onto SiO_2 (285 nm)/Si substrates using a water-assisted transfer method as explained in Figure S1 in the Supporting Information. The optical microscopy images (Figure 1c) show the MoS_2 thin film grown on sapphire (green) and the transferred film on SiO_2/Si (purple). Figure 1d shows MoS_2 and WS_2 thin films grown on a 2 in. sapphire wafer. The homogeneous contrast confirms the high quality and continuity of the MoS_2 and WS_2 films, maintained even after transfer. Raman spectra at specific locations on the as-grown wafer and together with Raman mapping, were measured to verify uniformity (Figure 1e and Figure S2 in the Supporting Information). Note that MoS_2 and WS_2 thin films exhibit a Raman difference between the E^1_{2g} and A_{1g} vibration modes of 23.2 and 61 cm^{-1}, respectively; this is consistent with previous reports on Raman of few-layer MoS_2 and WS_2.[32,33] All the measured Raman spectra have the same peak positions and similar peak intensity regardless of the measurement locations. These results indicate high spatial uniformity of the sulfurization process for few-layer MoS_2 and WS_2 films at wafer scales.

Figure 2a shows the sulfurization temperature profile versus processing time for the optimized sulfurization recipe. The evaporated 1.5 nm molybdenum and 1 nm tungsten metallic films on sapphire were heated up to 550 °C and this temperature was held for a dwell time of 15 min to achieve complete sulfurization. To achieve crystalline horizontally layered few-layer MoS_2 and WS_2 films at wafer scales a set of experiments was designed to optimize the sulfurization recipe. The effect of sulfurization parameters such as time, temperature and metal

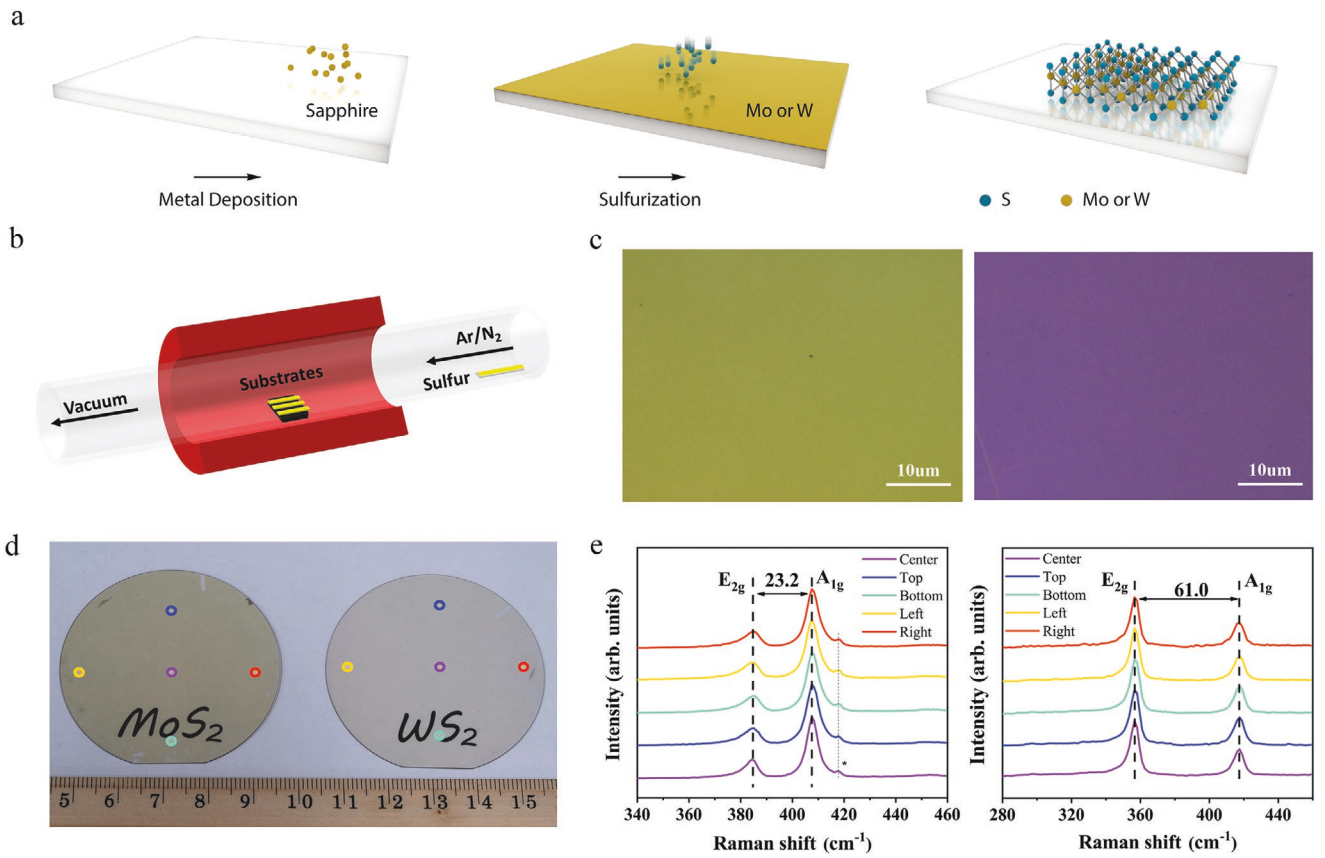

Figure 1. Large area MoS_2 and WS_2 thin film synthesis and their vibrational properties. a) Schematic illustration of the synthesis process for MoS_2 and WS_2 thin films: metallic Mo or W is deposited on the sapphire substrate followed by exposure to a sulfur-rich environment. b) Schematic of the furnace set up used for sulfurization. c) Optical images of the as-grown large-area MoS_2 on sapphire and on SiO_2 (285 nm)/Si. d) Optical images of MoS_2 and WS_2 grown on 2 in. sapphire (0001) wafers. e) Raman spectra of MoS_2 and WS_2 thin films taken at the points marked in Figure 1d (asterisk denotes the vibration mode from the sapphire substrate).

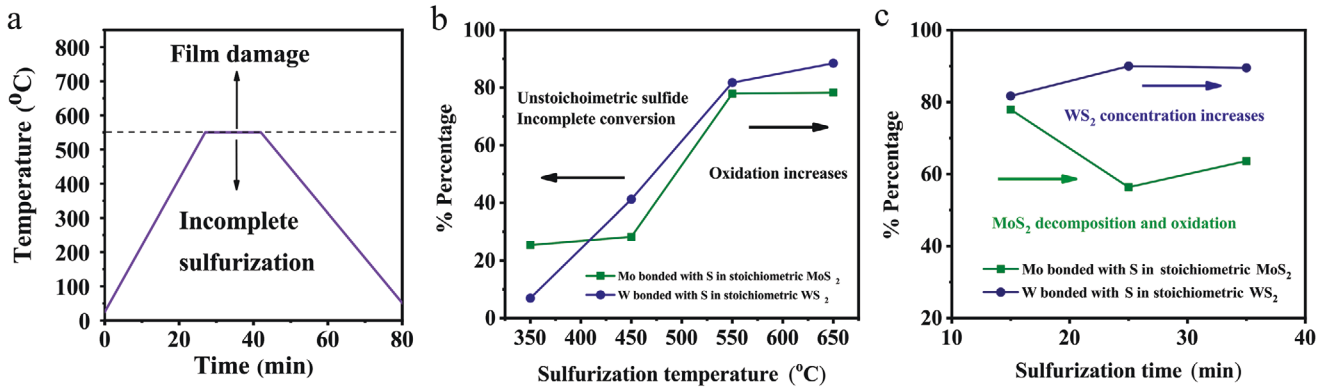

Figure 2. Tuning and optimization of sulfurization process. a) Temperature versus time profile of the sulfurization process. b) The percentage of Mo and W bonded with sulfur in stoichiometric MoS_2 and WS_2 versus temperature. c) The percentage of Mo and W bonded sulfur in stoichiometric MoS_2 and WS_2 versus sulfurization time. The optimized sulfurization process with a 15 min dwell time at a temperature of 550 °C leads to a high concentration of the stoichiometric sulfides with the least oxidation.

precursor thickness (discussed in TEM section), on the crystallinity and structure of sulfurized films was investigated systematically. First, time and temperature parameters were varied and the film quality/composition was analyzed by Raman and X-ray photoelectron spectroscopy (XPS). Four different temperatures of 350, 450, 550, and 650 °C were chosen, with a constant sulfurization dwell time of 15 min. Raman spectra of MoS_2 and WS_2 thin films sulfurized at different temperatures suggest a transition from incomplete sulfurization to more complete sulfurization, i.e., an improvement on crystallinity with increasing temperature, as indicated by the increasing peak intensity (compared to the sapphire peak) and the reduction of full-width at half maximum (FWHM) (Figure S3a in the Supporting Information). Figure 2b shows the percentage of Mo and W bonded with sulfur in stoichiometric MoS_2 and WS_2, based on XPS investigations (Figure S4 in the Supporting Information). It is worthwhile to note that the metallic precursors were found to transform to Mo and W bonded with S in stoichiometric MoS_2 and WS_2, Mo and W bonded with S in substoichiometric MoS_2 and WS_2, and Mo and W bonded with oxygen in superficial oxides, at all temperatures (350, 450, 550, and 650 °C) at different percentages. Meanwhile, the metallic Mo and W were not found in the resulting thin films synthesized at all temperatures. Mo and W are mostly bonded with S in unstoichiometric MoS_2 and WS_2 at lower temperatures (350 and 450 °C), while and at 550 °C an 80% of Mo and W are bonded with S in stoichiometric MoS_2 and WS_2. This indicates that a more complete sulfurization is achieved at 550 °C, consistent with the Raman results. Both Raman and XPS analysis show that percentage of stoichiometric MoS_2 and WS_2 and the crystallinity in the thin films increased with temperature (from 550 to 650 °C). However, the XPS analysis also shows an increasing existence of oxidized species with less sulfur species at temperatures over 550 °C (Figure S4, Supporting Information). Therefore, 550 °C was chosen as the optimum temperature that leads to a high concentration of the stoichiometric sulfides with the least oxidation. Then, the dwell time (15, 25, and 35 min) was evaluated with constant temperature of 550 °C. The resulting Raman spectra show similar fingerprint vibration modes of MoS_2 and WS_2 for all the studied sulfurization times (Figure S3b in the Supporting Information). Figure 2c shows the percentage of Mo and W bonded with S in stoichiometric MoS_2 and WS_2 as a function of dwell time, calculated from XPS analysis. The dwell time experiments further show that while WS_2 maintains its concentration at longer sulfurization times, MoS_2 tends to degrade and oxidize when the temperature was held for longer than 15 min (Figure S5 in the Supporting Information). Therefore, the optimized sulfurization process for Mo and W to transition to sulfides requires a 15 min dwell time at a temperature of 550 °C. All the compositional calculations in XPS analysis were calculated as reported elsewhere.[34–37]

Cross-section Transmission electron microscopy (TEM) was used to evaluate the structure of the thin films processed at 15 min and 550 °C. **Figure 3**a,b shows that both MoS_2 and WS_2 thin films are layered and crystalline. A capping layer was deposited above the thin films to avoid ion beam damage during the sample preparation. The thicknesses of films are estimated to be 1.92 and 1.32 nm for MoS_2 and WS_2, respectively. The interlayer spacing measured from TEM images is 6.4 and 6.6 Å, for both MoS_2 and WS_2, respectively, consistent with previous reports.[38,39] In contrast, thick Mo metallic precursors (25 nm) resulted in vertically and randomly aligned MoS_2 films, and thick W metallic precursors (10 nm) rendered wavy WS_2 films, as shown in Figure S6 in the Supporting Information, which is congruent with previous reports.[29] Therefore, the thickness of the deposited metallic precursor is a critical parameter that significantly impacts the orientation of the resulting sulfurized films.

The horizontally layered thin films processed at 15 min and 550 °C were also carefully examined by XPS (Figure 3c). For MoS_2 films, the binding energies for the doublets Mo $3d^{5/2}$ and $3d^{3/2}$ are 229.5 and 232.6 eV (blue bands), and for S $2p^{3/2}$ and $2p^{1/2}$ are 162.4 and 163.6 eV.[40] For WS_2 films, the binding energy for W $4f^{7/2}$ and $4f^{5/2}$ are 33.1 and 35.28 eV (blue bands), and those for S $2p^{3/2}$ and $2p^{1/2}$ are 162.7 and 163.8 eV.[41] These results are compatible with the corresponding binding energies for S 2p, Mo 3d, and W 4f in bulk MoS_2 and WS_2. The absence of Mo^0 $3d^{5/2}$,[42] and W^0 $4f^{7/2}$,[43] indicates complete sulfurization of the metallic film precursor. Low-intensity peaks representing bonds of Mo—O (red), W—O (orange), and S—S (green) bonds

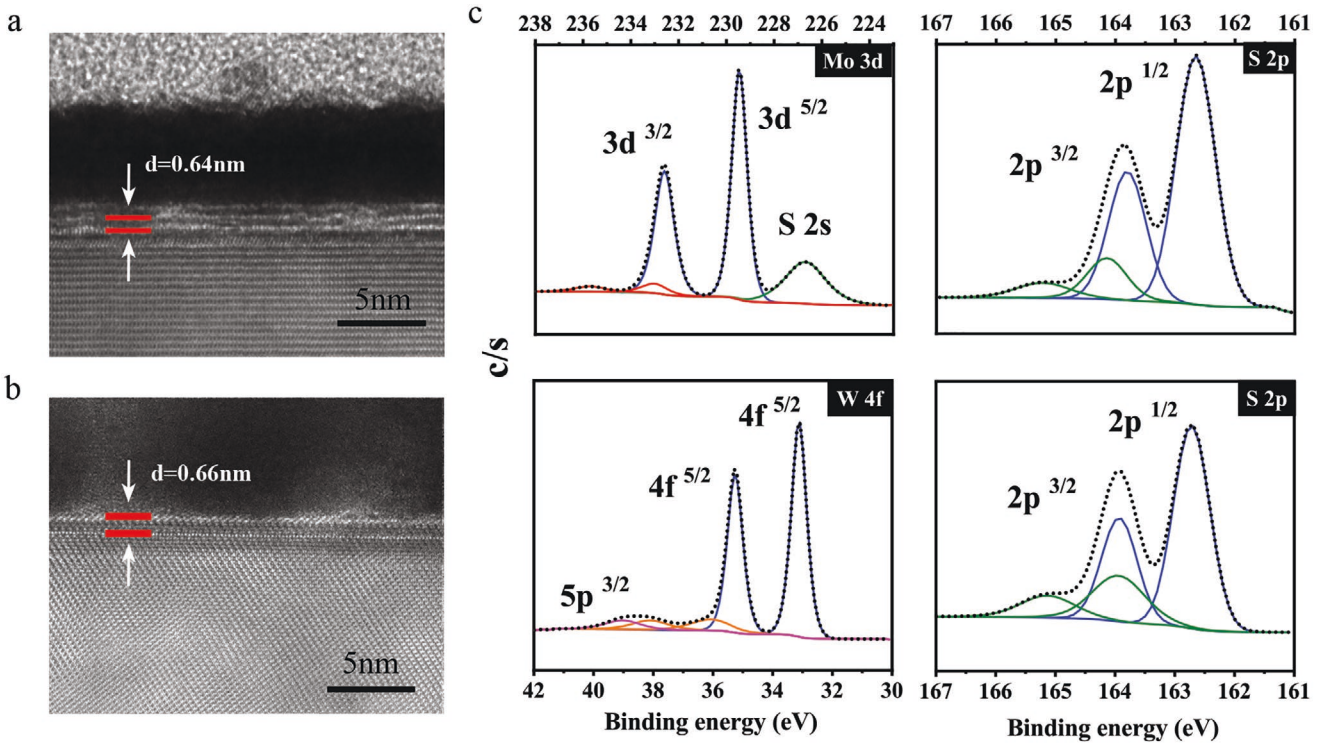

Figure 3. Evaluation of process optimized thin films. TEM cross-section of thin a) MoS_2 and b) WS_2 films. c) XPS spectra of Mo 3d, W 4f, and S 2p regions (MoS_2 top, WS_2 bottom) from sulfurized Mo and W films.

were also observed. This is probably due to the remaining oxygen and sulfur from the limitations of vacuum levels in our system. The presence of similar S-S or residual sulfur was also reported by Matsuura et al.,[44] even after sulfurization on the surface of sputtered Mo thin films. For this reason, future research may adopt a higher vacuum environment and longer evacuation time to improve the quality of TMD thin films. The S-to-Mo and S-to-W ratios were determined from XPS as 2.10 and 2.6 for MoS_2 and WS_2, respectively, which are close to the ideal value of 2.

Small-scale crossbar devices (1–4 μm^2) were fabricated as shown in **Figure 4**a,b. The MoS_2/WS_2 films were transferred onto as-prepared SiO_2 (285 nm)/Si substrates with predeposited bottom electrodes (BEs), followed by the deposition of top electrodes (TEs). Gold electrodes, which are electrochemically inert were used to avoid oxidation at the interface. Electrical measurements (I-V characteristics) were performed on fabricated crossbar devices to identify programming thresholds. Figure 4c,d shows the typical bipolar resistance switching in the Au/MoS_2/Au and Au/WS_2/Au devices at ambient conditions. For sulfurized MoS_2 film, the pristine device is initially at a high resistance state (HRS), until the formation of "conductive points" in MoS_2 films which connect the top and bottom electrodes at 3.1 V. The device then reaches a low resistance state (LRS),[45] which is commonly referred to as a set process. By sweeping a negative voltage from 0 to −1.5 V, the device is switched from the LRS to the HRS at about 0.8 V, known as the reset process. Similar resistance switching was observed in the WS_2 based device, which is set at 4 V and reset at 1.6 V. Similar to the previous report on monolayer TMD-based memristors,[13] electro-forming process is not required for the sulfurized TMD film-based devices. Devices are considered to have been pre-formed in the fabrication process (deposition of TEs); the detailed switching mechanism will be discussed later. A large on/off current ratio of 10^3 for MoS_2 and 10^5 for WS_2 can normally be achieved through the resistance switching. Some of the devices can even reach a higher on/off ratio, as shown in Figure S7a,b in the Supporting Information (10^4 for MoS_2 and 10^6 for WS_2). A compliance current is applied during the SET process to avoid a permanent or hard breakdown, while no compliance current is applied during the RESET process. To further investigate the transport mechanism, the *I–V* curves during set and reset processes are analyzed in double logarithmic coordinates. For sulfurized MoS_2 film, the LRS in both set and reset process exhibit linear dependence with a slope of ≈1, indicating ohmic conduction behavior, as described in Figure 4e,f. HRS in both set and reset processes show a typical trap-controlled space charge limited current (SCLC) behavior, which is divided into three regions.[16,46] In the first region, the number of injected carriers is smaller than the intrinsic thermal carriers in the film with a low injecting level, thus ohmic conduction with a slope of ≈1 is observed. As the voltage increases (the second region), a large amount of carrier is injected into the MoS_2 film compared to the intrinsic thermal carriers, wherein the *I–V* curves follow Child's rule with a slope of ≈2. With higher injecting current density (the third region), the traps in the MoS_2 film are filled, and a massive number of injected carriers contribute to the typical traps-filled-limit (TFL) conduction behavior with a slope >2 or a steep slope.[46] These traps most likely originate from sulfur vacancies and grain boundaries in the sulfurized MoS_2 film.[13]

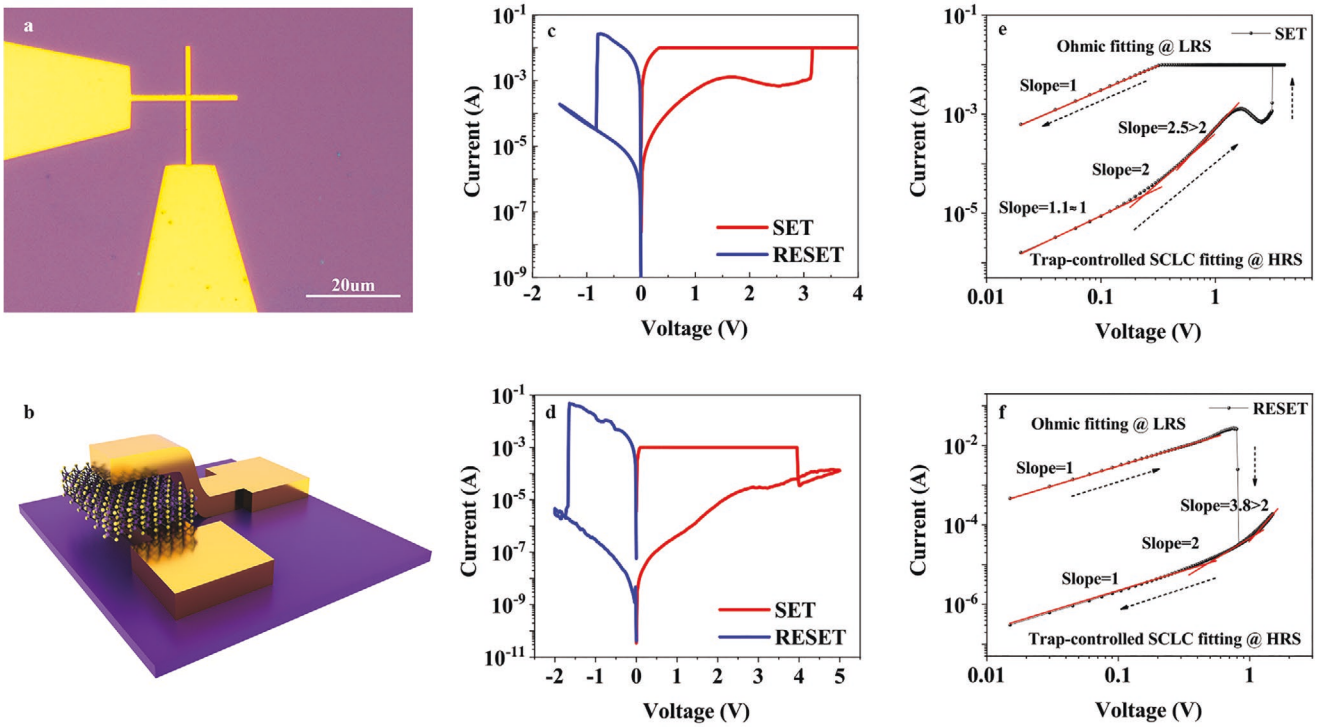

Figure 4. Memristors based on sulfurized MoS_2 and WS_2 thin films. a,b) Optical and schematic image of fabricated sulfurized film crossbar device with Au electrodes. Typical *I–V* curves of memristor devices based on sulfurized thin films. Representative *I–V* curves demonstrating unipolar resistive switching behavior in transferred c) MoS_2 film and d) WS_2 film crossbar device with lateral area of $1 \times 1\ \mu m^2$. Linear fitting (red line) for the *I–V* curves using double logarithmic coordinates. e) The set process and f) The reset process of MoS_2 memristor.

The fitting for WS_2 (Figure S7c,d in the Supporting Information) shows a similar trap-controlled SCLC behavior, which can be understood accordingly.

The retention and cyclicity of resistance switching behavior of memristors based on MoS_2 sulfurized at 550 °C was evaluated, shown in **Figure 5**a,b. The preliminary reliability tests show that the resistance states can be retained for more than 6 h at ambient condition and switching 30 manual DC cycles can be achieved. Our material characterization results suggest that sulfurization parameters (temperature and metal precursor thickness) have a significant influence on film quality and thus electrical properties, indicating additional approaches to improve the performance of memristors by optimizing the sulfurization process. To provide more insight on the effects of sulfurization parameters on memristor performance, memristors fabricated from MoS_2, synthesized at different sulfurization temperatures and with metal precursor thicknesses, were measured. To exclude the device-to-device variation, we carefully examined the arrays of sulfurized MoS_2 memristors, as shown in Figure S8 in the Supporting Information. First, MoS_2 thin films sulfurized with 1 nm/1.5 nm/2.5 nm Mo precursor at 550 °C, as T1, T2, and T3, were firstly studied, and Atomic Force Microscope (AFM) was employed to reveal thin film thickness (Figure S9 in the Supporting Information). Figure 5c shows that memristors based on MoS_2 with different thicknesses have a similar range of SET and RESET, suggesting a thickness-independent switching mechanism. Meanwhile, yield and endurance tests (Figure 5d) show a consistent trend of improvement with the increasing thickness (from T1 to T3). A remarkably high yield of over 90% was observed for T3, and high DC cycling (above 120 cycles) was reached, as shown in Figure S10 in the Supporting Information. Then, we studied MoS_2 thin films sulfurized with 1.5 nm Mo precursor at different temperatures (350, 550, and 650 °C). Figure 5c,d shows a significant improvement in SET voltage (≈1 V reduction) with a very narrow distribution range and enhancement on yield and endurance, from 550 to 650 °C, while 350 °C surprisingly shows a mild performance. All these experimental observations prove that tuning the sulfurization parameters (temperature/metal precursor thickness) is a simple yet efficacious approach enhance the performance of memristors. With different sulfurization methods, the properties of MoS_2/WS_2 film are different, leading to a variation in the performance of the memristor. Table S1 (Supporting Information) summarizes the memristor-based sulfurized TMD films published in the literature.

Recent MoS_2 contact studies have shown that broken layers or metal diffusion can occur during metal deposition,[47–49] while another scanning tunneling microscope (STM) study has shown that sulfur vacancies play a critical role in resistive switching in monolayer MoS_2.[50] To understand the improvement from increasing the thickness and temperature (from 550 to 650 °C), a qualitative model is proposed based on these previous experimental observations, as shown in Figure 5g. Broken layers or metal diffusion (in black box) and sulfur vacancies for Au substitution (in red box), are considered as the two major types of defects that determine the performance of memristors. With increasing thickness, there is less chance that broken layers or metal diffusion would occur in MoS_2 thin films,

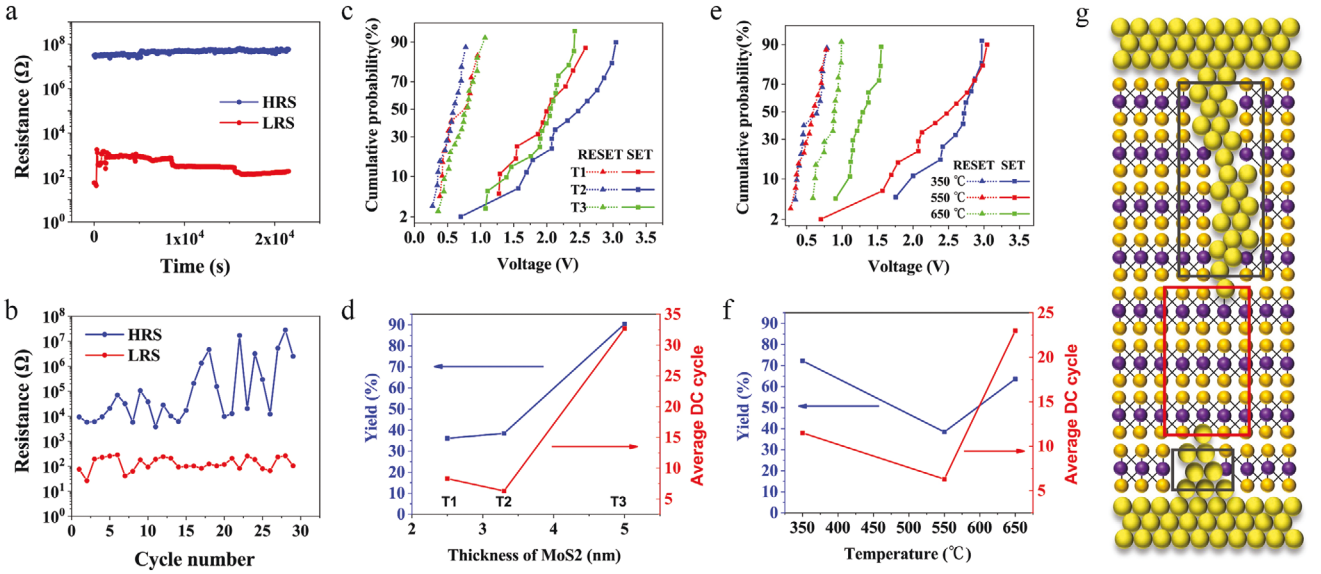

Figure 5. Reliability characterizations of sulfurized MoS_2 based memristors. a) The retention time of sulfurized MoS_2 memory devices stable over 6 h at ambient condition. b) Endurance of sulfurized MoS_2 memristor device with 30 manual DC switching cycles. SET and RESET voltage distribution, yield and endurance with MoS_2 sulfurized with different parameters. c) SET and RESET voltage distribution of MoS_2 sulfurized with different Mo precursor thicknesses (T1/T2/T3:1/1.5/2.5 nm). d) Yield and endurance of MoS_2 with different thicknesses. A remarkable high yield (over 90%) can be achieved with T3. e) SET and RESET voltage distribution of MoS_2 sulfurized at different temperatures. A significant reduction and narrow distribution of SET voltage is achieved with 650 °C. f) yield and endurance of MoS_2 at different temperatures. g) Illustration of defects in MoS_2 film (layer broken in black box and sulfur vacancies with Au substitution in red box).

leading to device failure. These broken layers are also considered as the main reason why unusual forming free behavior was observed for multilayer MoS_2. Resistive switching is attributed to local Au substitution at sulfur vacancies where layer breaking ceases, which is independent of film thickness. The crystallinity of MoS_2 thin films improves with increasing presence of oxidized species while temperature is increased from 550 to 650 °C, as discussed before. This suggests less broken layers, but more substitutable vacancies for Au atoms for the MoS_2 films sulfurized at 650 °C. This is consistent with yield enhancement. Additionally, the presence of more substitutable vacancies implies that less electric field stress is required for switching, thus reducing set voltage and a narrower set voltage distribution range.

3. Conclusion

In conclusion, we demonstrate a simple method to synthesize large-area few-layer MoS_2 and WS_2 via a one-step low-temperature sulfurization process. The quality of the resulting sulfurized thin films depends directly on the accurate control of the sulfurization temperature, time, and thickness of the metallic precursors. The optimized sulfurization process with a 15 min dwell time at a temperature of 550 °C leads to a high concentration of the stoichiometric sulfides with the least oxidation. The sulfurized film-based memristors show stable non-volatile switching and a satisfactory on/off current ratio (10^3–10^5). A remarkable high yield (over 90%) enhancement is achieved with increasing film thickness, and a significant reduction and narrow distribution of SET voltage is achieved by increasing the sulfurization temperature to 650 °C (from 550 °C). This shows that tuning the sulfurization parameters (temperature and metal precursor thickness) is a direct method to improve the electrical characteristics of memristors.

4. Experimental Section

Thin-Film Synthesis: First, C-plane <0001> sapphire substrates were cleaned using acetone, isopropanol and then dried. Then, the substrates were introduced to the electron beam evaporation chamber. The main chamber was evacuated up to a base pressure of 10^{-6} Torr, followed by a pre-evaporation of the Mo or W pellets to eliminate impurities from the precursors. All the high purity (>99.95%) metallic pellets were obtained commercially. Subsequently, the shutter was opened, and the metal (Mo or W) was deposited at a rate of 0.1 Å s^{-1}. After the metal evaporation, the as-obtained metallic films were stored in a vacuum box before sulfurization. The thickness of the evaporated thin films was confirmed with AFM.

A three-zone tube furnace (base pressure of 10^{-1} Pa) was used for the sulfurization process. First, the furnace was purged with N_2 gas to remove impurities in the tube, then pumped down again to the base pressure. Then, the metallic (W or Mo) films were introduced in the center of the tube and the sulfurization process was carried out in an Argon atmosphere (32 Pa). The quartz tube was heated to 550 °C; this temperature was held for 15 min. Simultaneously, the sulfur powder (99.5–100.5% from Sigma-Aldrich) was placed upstream and heated up to 200 °C during the sulfurization process. Finally, the films were rapidly cooled down to room temperature.

Film Characterization: Raman spectra were acquired using a Renishaw InVia equipped with two lasers, at 532 nm for MoS_2 and 442 nm for WS_2 at atmospheric conditions. The laser powers were less than 1 mW during the measurements. The MoS_2 and WS_2 thin films were analyzed using a Kratos X-ray Photoelectron Spectrometer – Axis Ultra DLD with a Silver anode beam to irradiate the sample surface. The samples were analyzed at a 45° take-off angle between the sample surface and the path to the analyzer, and a charge neutralization was performed by irradiating low-energy

electrons. The Gaussian-Lorentz mixed function was employed for peak deconvolution in XPS analysis. The thickness of the film is measured using a Bruker's Dimension Icon AFM system with ScanAsyst mode.

Transmission Electron Microscopy: Cross-section TEM foil was prepared using a ThermoScientific Helios NanoLab 600 Gallium FIB/SEM. The sample was initially coated with Au using an EMS/Quorum 150R. An additional Pt coating layer (≈2 µm) was added prior to milling. Lift out of the prepared thick foil was placed in a half grid and milled with 30 and 16 kV until a thickness of ≈50 nm. Final polishing was done at 2 kV until reaching a nominal thickness of 30 nm. The sample was purposely prepared thicker than conventional foils to prevent fast degradation of the interface during imaging. TEM images were acquired in an image corrected FEI Titan 80–300 operating at 300 kV and equipped with a Gatan OneView camera.

Device Fabrication and Measurement: Electron beam lithography was used to pattern bottom electrodes (BE) of crossbar devices followed by 2 nm Cr/60 nm Au metal deposition on a SiO_2 (285 nm)/Si substrate. Sulfurized MoS_2 (or WS_2) films were then transferred onto the fabricated substrate using a water-assisted transfer method (details in Supporting Information). The polymer used in transfer was carefully removed by immersing the samples in toluene for 24–48 h. Top electrodes (TE), using the same fabrication process as BE, were patterned, and deposited. The DC characteristics of the devices were taken on a Cascade probe station with an Agilent 4156 semiconductor parameter analyzer under ambient conditions.

Supporting Information

Supporting Information is available from the Wiley Online Library or from the author.

Acknowledgements

Y.G. and M.I.S. contributed equally to this work. This research was primarily supported by the National Science Foundation through the Center for Dynamics and Control of Materials: an NSF MRSEC under Cooperative Agreement No. DMR-1720595. The work was partly done at the Texas Nanofabrication Facility supported by NSF grant NNCI-2025227. This work was performed in part at the Center for Integrated Nanotechnologies, an Office of Science User Facility operated for the U.S. Department of Energy (DOE) Office of Science. Los Alamos National Laboratory, an affirmative action equal opportunity employer, is managed by Triad National Security, LLC for the U.S. Department of Energy's NNSA, under contract 89233218CNA000001. The authors acknowledge Jo Wozniak of Texas Advanced Computing Centre (TACC) for 3D renderings.

Conflict of Interest

The authors declare no conflict of interest.

Data Availability Statement

The data that supports the findings of this study are available in the supplementary material of this article.

Keywords

2D materials, resistive switching, sulfurization, thin-film processing

Received: May 18, 2021
Revised: August 20, 2021
Published online: October 7, 2021

[1] D. Akinwande, C. Huyghebaert, C.-H. Wang, M. I. Serna, S. Goossens, L.-J. Li, H.-S. P. Wong, F. H. L. Koppens, *Nature* **2019**, *573*, 507.
[2] D. Ielmini, H.-S. P. Wong, *Nat. Electron.* **2018**, *1*, 333.
[3] S. B. Desai, S. R. Madhvapathy, A. B. Sachid, J. P. Llinas, Q. Wang, G. H. Ahn, G. Pitner, M. J. Kim, J. Bokor, C. Hu, H.- S. P. Wong, A. Javey, *Science* **2016**, *354*, 99.
[4] P. Zhao, A. Azcatl, Y. Y. Gomeniuk, P. Bolshakov, M. Schmidt, S. J. McDonnel, C. L. Hinkle, P. K. Hurley, R. M. Wallace, C. D. Young, *ACS Appl. Mater. Interfaces* **2017**, *9*, 24348.
[5] G.-S. Kim, S.-H. Kim, J. Park, K. H. Han, J. Kim, H.-Y. Yu, *ACS Nano* **2018**, *12*, 6292.
[6] E. Singh, P. Singh, K. S. Kim, G. Y. Yeom, H. S. Nalwa, *ACS Appl. Mater. Interfaces* **2019**, *11*, 11061.
[7] J. Yoon, W. Park, G.-Y. Bae, Y. Kim, H. S. Jang, Y. Hyun, S. K. Lim, Y. H. Kahng, W.-K. Hong, B. H. Lee, H. C. Ko, *Small* **2013**, *9*, 3185.
[8] T.-H. Tsai, Z.-Y. Liang, Y.-C. Lin, C.-C. Wang, K.-I. Lin, K. Suenaga, P.-W. Chiu, *ACS Nano* **2020**, *14*, 4559.
[9] O. Lopez-Sanchez, D. Lembke, M. Kayci, A. Radenovic, A. Kis, *Nat. Nanotechnol.* **2013**, *8*, 497.
[10] H. Y. Jeong, J. Y. Kim, J. W. Kim, J. O. Hwang, J.-E. Kim, J. Y. Lee, T. H. Yoon, B. J. Cho, S. O. Kim, R. S. Ruoff, S.-Y. Choi, *Nano Lett.* **2010**, *10*, 4381.
[11] A. A. Bessonov, M. N. Kirikova, D. I. Petukhov, M. Allen, T. Ryhänen, M. J. A. Bailey, *Nat. Mater.* **2015**, *14*, 199.
[12] C. Tan, Z. Liu, W. Huang, H. Zhang, *Chem. Soc. Rev.* **2015**, *44*, 2615.
[13] R. Ge, X. Wu, M. Kim, J. Shi, S. Sonde, L. Tao, Y. Zhang, J. C. Lee, D. Akinwande, *Nano Lett.* **2018**, *18*, 434.
[14] X. Wu, R. Ge, P.-A. Chen, H. Chou, Z. Zhang, Y. Zhang, S. Banerjee, M. -. H. Chiang, J. C. Lee, D. Akinwande, *Adv. Mater.* **2019**, *31*, 1806790.
[15] M. Kim, R. Ge, X. Wu, X. Lan, J. Tice, J. C. Lee, D. Akinwande, *Nat. Commun.* **2018**, *9*, 1.
[16] R. Xu, H. Jang, M.-H. Lee, D. Amanov, Y. Cho, H. Kim, S. Park, H.-J. Shin, D. Ham, *Nano Lett.* **2019**, *19*, 2411.
[17] H. Zhao, Z. Dong, H. Tian, D. Dimarzi, M.-G. Han, L. Zhang, X. Yan, F. Liu, L. Shen, S.-J. Han, S. Cronin, W. Wu, J. Tice, J. Guo, H. Wang, *Adv. Mater.* **2017**, *29*, 1703232.
[18] M. Kim, E. Pallecchi, R. Ge, X. Wu, G. Ducournau, J. C. Lee, H. Happy, D. Akinwande, *Nat. Electron.* **2020**, *3*, 479.
[19] H. Yu, M. Liao, W. Zhao, G. Liu, X. J. Zhou, Z. Wei, X. Xu, K. Liu, Z. Hu, K. Deng, S. Zhou, J.-A. Shi, L. Gu, C. Shen, T. Zhang, L. Du, L. Xie, J. Zhu, W. Chen, R. Yang, D. Shi, G. Zhang, *ACS Nano* **2017**, *11*, 12001.
[20] X. Xu, G. Das, X. He, M. N. Hedhili, E. D. Fabrizio, X. Zhang, H. N. Alshareef, *Adv. Funct. Mater.* **2019**, *29*, 1901070.
[21] H. Yang, A. Giri, S. Moon, S. Shin, J.-M. Myoung, U. Jeong, *Chem. Mater.* **2017**, *29*, 5772.
[22] Y. Guo, P.-C. Shen, C. Su, A.-Y. Lu, M. Hempel, Y. Han, Q. Ji, Y. Lin, E. Shi, E. Mcvay, L. Dou, D. A. Muller, T. Palacios, J. Li, X. Ling, J. Kong, *Proc. Natl. Acad. Sci. USA* **2019**, *116*, 3437.
[23] X. Chen, Y. J. Park, T. Das, H. Jang, J.-B. Lee, J.-H. Ahn, *Nanoscale* **2016**, *8*, 15181.
[24] L. Lin, J. Li, W. Li, M. N. Yogeesh, J. Shi, X. Peng, Y. Liu, B. B. Rajeeva, M. F. Becker, Y. Liu, D. Akinwande, Y. Zheng, *Adv. Funct. Mater.* **2018**, *28*, 1803990.
[25] J. Zhou, J. Lin, X. Huang, Y. Zhou, Y. Chen, J. Xia, H. Wang, Y. Xie, H. Yu, J. Lei, D. Wu, F. Liu, Q. Fu, Q. Zeng, C.-H. Hsu, C. Yang, L. Lu, T. Yu, Z. Shen, H. Lin, B. I. Yakobson, Q. Liu, K. Suenaga, G. Liu, Z. Liu, *Nature* **2018**, *556*, 355.
[26] H. Cun, M. Macha, H. Kim, K. Liu, Y. Zhao, T. Lagrange, A. Kis, A. Radenovic, *Nano Res.* **2019**, *12*, 2646.
[27] K. Kang, S. Xie, L. Huang, Y. Han, P. Y. Huang, K. F. Mak, C.-J. Kim, D. Muller, J. Park, *Nature* **2015**, *520*, 656.
[28] D. Kong, H. Wang, J. J. Cha, M. Pasta, K. J. Koski, J. Yao, Y. Cui, *Nano Lett.* **2013**, *13*, 1341.
[29] Y. Jung, J. Shen, Y. Liu, J. M. Woods, Y. Sun, J. J. Cha, *Nano Lett.* **2014**, *14*, 6842.

[30] C.-R. Wu, X.-R. Chang, C.-H. Wu, S.-Y. Lin, *Sci. Rep.* **2017**, *7*, 1.
[31] J. Park, N. Choudhary, J. Smith, G. Lee, M. Kim, W. Choi, *Appl. Phys. Lett.* **2015**, *106*, 012104.
[32] C. Lee, H. Yan, L. E. Brus, T. F. Heinz, J. Hone, S. Ryu, *ACS Nano* **2010**, *4*, 2695.
[33] W. Zhao, Z. Ghorannevis, K. K. Amara, J. R. Pang, M. Toh, X. Zhang, C. Kloc, P. H. Tan, G. Eda, *Nanoscale* **2013**, *5*, 9677.
[34] http://www.casaxps.com/help_manual/manual_updates/Basics_Quantification_of_XPS_Spectra.pdf.
[35] R. Amin, M. A. Hossain, Y. Zakaria, *ACS Appl. Mater. Interfaces* **2018**, *10*, 13509.
[36] M. Z. Xie, J. Y. Zhou, H. Ji, Y. Ye, X. Wang, K. Jiang, L. Y. Shang, Z. G. Hu, J. H. Chu, *Appl. Phys. Lett.* **2019**, *115*, 121901.
[37] X. Zhao, X. Ma, J. Sun, D. Li, X. Yang, *ACS Nano* **2016**, *10*, 2159.
[38] B. Radisavljevic, A. Radenovic, J. Brivio, V. Giacometti, A. Kis, *Nat. Nanotechnol.* **2011**, *6*, 147.
[39] D. Ovchinnikov, A. Allain, Y.-S. Huang, D. Dumcenco, A. Kis, *ACS Nano* **2014**, *8*, 8174.
[40] A. Levasseur, P. Vinatier, D. Gonbeau, *Bull. Mater. Sci.* **1999**, *22*, 607.
[41] G. Huang, H. Liu, S. Wang, X. Yang, B. Liu, H. Chen, M. Xu, *J. Mater. Chem. A* **2015**, *3*, 24128.
[42] P. A. Spevack, N. S. Mcintyre, *J. Phys. Chem.* **1993**, *97*, 11031.
[43] C. Wagner, NIST: NIST X-ray Photoelectron Spectroscopy Database Version 1.0. *Office of Standard Reference Data*, National Institute of Standards and Technology (NIST), Gaithersburg, MD **1989**.
[44] K. Matsuura, T. Ohashi, I. Muneta, S. Ishihara, K. Kakushima, K. Tsutsui, A. Ogura, H. Wakabayashi, *J. Electron. Mater.* **2018**, *47*, 3497.
[45] R. Ge, X. Wu, L. Liang, S. M. Hus, Y. Gu, E. Okogbue, H. Chou, J. Shi, Y. Zhang, S. K. Banerjee, Y. Jung, J. C. Lee, D. Akinwande, *Adv. Mater.* **2021**, *33*, 2007792.
[46] M. A. Lampert, *Phys. Rev.* **1956**, *103*, 1648.
[47] Y. Liu, J. Guo, E. Zhu, L. Liao, S.-J. Lee, M. Ding, I. Shakir, V. Gambin, Y. Huang, X. Duan, *Nature* **2018**, *557*, 696.
[48] L. Liu, L. Kong, Q. Li, C. He, L. Ren, Q. Tao, X. Yang, J. Lin, B. Zhao, Z. Li, Y. Chen, W. Li, W. Song, Z. Lu, G. Li, S. Li, X. Duan, A. Pan, L. Liao, Y. Liu, *Nat. Electron.* **2021**, *4*, 342.
[49] Y. Jung, M. S. Choi, A. Nipane, A. Borah, B. Kim, A. Zangiabadi, T. Taniguchi, K. Watanabe, W. J. Yoo, J. Hone, J. T. Teherani, *Nat. Electron.* **2019**, *2*, 187.
[50] S. M. Hus, R. Ge, P.-A. Chen, L. Liang, G. E. Donnelly, W. Ko, F. Huang, M.-H. Chiang, A.-P. Li, D. Akinwande, *Nat. Nanotechnol.* **2021**, *16*, 58.